Monthly Notices of the ROYAL ASTRONOMICAL SOCIETY

MNRAS **506,** 6111–6116 (2021) https://doi.org/10.1093/mnras/stab1296
Advance Access publication 2021 May 11

Kepler's Goat Herd: An exact solution to Kepler's equation for elliptical orbits

Oliver H. E. Philcox [1,2★] Jeremy Goodman[1] and Zachary Slepian[3,4]

[1]*Department of Astrophysical Sciences, Princeton University, Princeton, NJ 08540, USA*
[2]*School of Natural Sciences, Institute for Advanced Study, 1 Einstein Drive, Princeton, NJ 08540, USA*
[3]*Department of Astronomy, University of Florida, 211 Bryant Space Science Center, Gainesville, FL 32611, USA*
[4]*Physics Division, Lawrence Berkeley National Laboratory, 1 Cyclotron Road, Berkeley, CA 94709, USA*

Accepted 2021 May 3. Received 2021 April 29; in original form 2021 March 29

ABSTRACT

A fundamental relation in celestial mechanics is Kepler's equation, linking an orbit's mean anomaly to its eccentric anomaly and eccentricity. Being transcendental, the equation cannot be directly solved for eccentric anomaly by conventional treatments; much work has been devoted to approximate methods. Here, we give an explicit integral solution, utilizing methods recently applied to the 'geometric goat problem' and to the dynamics of spherical collapse. The solution is given as a ratio of contour integrals; these can be efficiently computed via numerical integration for arbitrary eccentricities. The method is found to be highly accurate in practice, with our C++ implementation outperforming conventional root-finding and series approaches by a factor greater than two.

Key words: methods: analytical – methods: numerical – celestial mechanics.

1 INTRODUCTION

Kepler's equation states that

$$E - e\sin E = \ell \tag{1}$$

for eccentric anomaly $E \in [0, 2\pi)$, eccentricity $e \in [0, \infty)$ and mean anomaly $\ell \in [0, 2\pi)$ (often denoted M). This describes the dynamics of a two-body system, and was first published over 400 yr ago (Kepler 1609). It is most commonly applied to (non-circular) elliptical orbits, whereupon $0 < e < 1$. Assuming such an orbit, the quantities in (1) may be related to other orbital parameters of interest via

$$\ell = n(t-\tau), \quad x = a(\cos E - e), \quad y = a\sqrt{1-e^2}\sin E \tag{2}$$

(Murray & Dermott 1999), with $t - \tau$ being the time-coordinate relative to pericentre crossing, n the mean motion, a the semimajor axis, and (x, y) the Cartesian positions in the orbital plane, relative to the centre of the ellipse. A solution of (1) thus specifies the full location of the orbiting body as a function of time.

Despite its age, Kepler's equation is no less relevant today than in 1609; it still appears in many contexts, with crucial examples including Global Positioning System (GPS) calibration and the determination of satellite and debris positions by the United States Space Surveillance Network (SSN).[1] Being a transcendental equation, conventional methods cannot solve (1) directly, which has led to a vast literature concerning alternative approaches, such as root-finding and series solutions. Indeed, Colwell (1993) notes that new methods of solution have been proposed in almost every decade since 1650. Below, we present our contribution to this canon.

Before discussing Kepler's equation in detail, we briefly mention a seemingly unrelated topic: the 'geometric goat problem'. Roughly speaking, the problem is the following: 'Imagine a goat is tied to the edge of a circular enclosure. How long must the rope be such that the goat can graze in exactly half of the field?' Recent work by Ullisch (2020) shows this to be equivalent to solving the transcendental equation $\sin\beta - \beta\cos\beta = \pi/2$ for β. Using methods drawn from complex analysis, Ullisch (2020) provides an explicit solution to the problem via a ratio of contour integrals, each of which can be easily computed using FFTs or direct summation. Given the similarity between this and (1), we may ask whether an analogous solution is possible in our case. Further support for this approach is given by Slepian & Philcox (2021), which used the same methods to explicitly solve the spherical collapse equations, which are a special case of (1) with $e = 1$.

The remainder of this paper is structured as follows. In Section 2, we present the explicit solution of Kepler's equation, alongside a proof of its validity, before discussing its practical evaluation in Section 3. Discussion of alternative solution methods is provided in Section 4 before a comparison is made in Section 5 alongside our conclusions. All computations in this work were performed in C++ and plotted using PYTHON.

2 INTEGRAL SOLUTION

Our first step is to demonstrate that (1) has a unique solution in the range of interest. We will assume that the eccentricity is both fixed and in the range $e \in (0, 1)$, i.e. that we have a non-circular elliptical orbit. Considering the function

$$g(E; e) \equiv E - e\sin E \tag{3}$$

★ E-mail: ohep2@cantab.ac.uk
[1]See www.space-track.org.

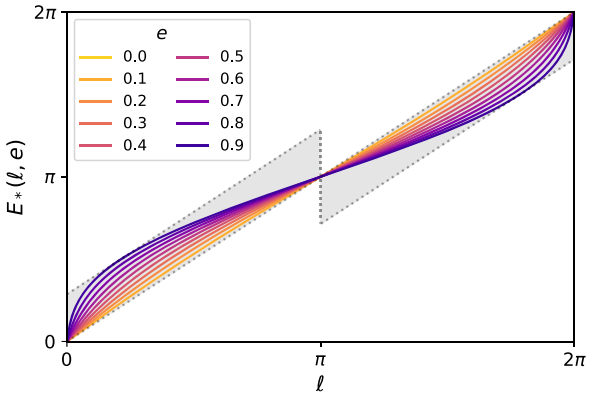

Figure 1. Solutions to Kepler's equation as a function of the mean anomaly ℓ for various values of the eccentricity e (shown in the legend). All results are obtained using the contour integration method of this work with 32 steps. The dotted lines show the functions $E = \ell$ and $E = \ell \pm e$; the solution for E lies in the light grey region between the two in all cases. As noted in Section 2, the solutions are symmetric about $\ell = \pi$.

the solution $E^*(\ell, e)$ satisfies $g(E_*(\ell, e); e) = \ell$. Given that $g(E; e)$ is an odd function of e, and (1) is invariant under $E \to E + 2\pi$, $\ell \to \ell + 2\pi$, we need only consider the range $\ell \in [0, \pi]$. We additionally avoid the trivial solutions $E = 0, \pi$ at $\ell = 0, \pi$.

Considering the end-points, $g(0; e) = 0$, $g(\pi; e) = \pi$; since the function is smooth, $g(E; \ell, e)$ must thus equal ℓ at least once for all $\ell \in (0, \pi)$. In fact $g(E; e)$ is monotonic in E for all $|e| < 1$, hence there is a single solution $E_*(\ell, e)$. This is easily shown by noting that both E and $e\sin E$ are zero at $E = 0$ and E increases faster than $|e\sin E|$ for all $|e| < 1$, hence $E > |e\sin E|$ everywhere. For reference, we provide a plot of the solution $E_*(\ell, e)$ for various values of e and ℓ in Fig. 1.

To define an integral solution to (1), we first consider the entire function f

$$f \;:\; U \to \mathbb{C}$$
$$f(z; \ell, e) = z - e\sin z - \ell \tag{4}$$

defined on a simply connected region $U = (0, 2\pi) \times i(-\infty, \infty)$ in the complex plane. The parameters e, ℓ take the values $e \in (0, 1)$ and $\ell \in (0, \pi)$ as before. Restricting to the real line, the solution to $f(z; \ell, e) = 0$, denoted $z_0(\ell, e)$, recovers Kepler's equation, in the sense that $z_0(\ell, e) \equiv E_*(\ell, e)$.

To proceed, we use the theorem of Ullisch (2020), as in Slepian & Philcox (2021) (and found previously in Jackson 1916, 1917; Luck & Stevens 2002; Luck, Zdaniuk & Cho 2015).[2] This states that, for an open simply connected subset U of $\mathbb{C}$ with a non-zero analytic function f defined therein, for each simple zero $z_0 \in U$ of f, there exists a closed curve $C \in U$ such that:

$$z_0 = \left[\oint_C \frac{z\,\mathrm{d}z}{f(z)}\right] \Big/ \left[\oint_C \frac{\mathrm{d}z}{f(z)}\right]. \tag{5}$$

(5) follows directly from the Residue Theorem under the assumptions stated: the numerator evaluates to $2\pi i z_0/\dot{f}(z_0)$, and the denominator to $2\pi i/\dot{f}(z_0)$. Furthermore, (5) holds for any Jordan curve $C \in U$, provided that (i) it encloses z_0, and (ii) $f(z) \neq 0$ at all points on C and its interior, except at $z = z_0$.

[2]An alternative solution using complex methods can be found in Siewert & Burniston (1972). Our approach is significantly more straightforward however.

In our context, $f(z) \equiv f(z, \ell, e)$ is defined by (4), and, provided certain conditions are met, we may use (5) to evaluate $z_0(\ell, e)$ and hence obtain $E_*(\ell, z)$. Below, we consider the conditions in detail:

(i) $\boldsymbol{z_0}$ **lies within** $\boldsymbol{U}$. By the discussion above, $f(z, \ell, e) = 0$ on the real-line at a single point with $z_0(\ell, e) = E_*(\ell, e)$. Since $E \in (0, \pi)$ (for $\ell \in (0, \pi)$), z_0 lies within U.

(ii) $\boldsymbol{z_0}$ **is a simple zero**. From (4), $\dot{f}(z) = 1 - e\cos z$, which for $e \in (0, 1)$, has no solutions on the real line. Thus $\dot{f}(z_0) \neq 0$, hence the zero at z_0 is simple.

(iii) $\boldsymbol{z_0}$ **is enclosed within** $\boldsymbol{C}$. A simple choice is to assume the (Jordan) circular contour $C = \{z: |z - \pi/2| < \pi/2 - \epsilon\}$ for small parameter $\epsilon > 0$ (analogous to Slepian & Philcox 2021). This intersects the real axis at $\mathrm{Re}[z] = \epsilon, \pi - \epsilon$; thus, for sufficiently small ϵ, z_0 is enclosed with C (for any choice of e and ℓ). In practice, we find a different contour to be more advantageous for efficient numerical implementation; this is discussed below.

(iv) $\boldsymbol{z_0}$ **is the** only **zero within** $\boldsymbol{C}$. To prove this, we first consider the region $\mathcal{R} \subset U$ defined by $\mathcal{R} = (0, 2\pi) \times i(-M, M)$ for large M. Since C lies within $\mathcal{R}$, the condition is satisfied if $f(z; \ell, e) \neq 0$ everywhere in $\mathcal{R}\backslash\{z_0\}$.[3] To prove this, we consider the variation in $\arg[f(z; \ell, e)]$ as one traverses the boundary $\partial\mathcal{R}$ in a counterclockwise fashion. Writing $z = (x + iy)$, $f(z; \ell, e)$ may be written $f(x, y; \ell, e) = (x - e\sin x\cosh y - \ell) + i(y - e\cos x\sinh y)$. Considering each part of the contour in turn, and taking $M \to \infty$:

(i) Moving from $z = 0 - iM$ to $z = 2\pi - iM$, we have $f(z; \ell, e) = (i/2)e\exp(M + ix) + \mathcal{O}(M)$, thus $\Delta\arg[f(z; \ell, e)] = +2\pi$.

(ii) From $z = 2\pi - iM$ to $2\pi + iM$, $f(z; \ell, e) = 2\pi - \ell + i(y - e\sinh y)$, thus $\mathrm{Re}[f(z; \ell, e)]$ is constant and positive, whilst $\mathrm{Im}[f(z; \ell, e)]$ moves from $(1/2)e\exp M$ to $-(1/2)e\exp M$, giving $\Delta\arg[f(z; \ell, e)] = -\pi$.

(iii) Similarly from $z = 2\pi + iM$ to $0 + iM$, $f(z; \ell, e) = -(i/2)e\exp(M - ix) + \mathcal{O}(M)$, thus $\Delta\arg[f(z; \ell, e)] = +2\pi$.

(iv) Finally, from $z = 0 + iM$ to $z = 0 - iM$, $f(z; \ell, e) = -\ell + i(y - e\sinh y)$, thus $\mathrm{Re}[f(z; \ell, e)]$ is constant and negative, whilst $\mathrm{Im}[f(z; \ell, e)]$ moves from $-(1/2)e\exp M$ to $(1/2)e\exp M$, giving $\Delta\arg[f(z; \ell, e)] = -\pi$.

Summing the contributions, we find $\Delta\arg[f(z; \ell, e)] = +2\pi$ when traversing the full closed contour $\partial\mathcal{R}$ in a counterclockwise fashion. From the argument principle, this is equal to $2\pi(Z - P)$, where Z and P are, respectively, the number of zeros and poles within $\mathcal{R}$. Since $P = 0$ (as neither z nor $\sin z$ contain any poles in $\mathbb{C}$), we find $Z = 1$, thus $\mathcal{R}$ contains only a single zero. This implies that z_0 is the only zero of $f(z; \ell, e)$ in $\mathcal{R}$, or, given that M is arbitrary, $f(z; \ell, e) \neq 0$ for all $z \in U\backslash\{z_0\}$.

It remains to choose the contour C. Whilst the large circle $C = \{z: |z - \pi/2| < \pi/2 - \epsilon\}$ is a valid choice, given that it lies within U and encloses z_0, for numerical efficiency it is preferred to use a smaller circular contour (cf. Section 3). To form this, we first consider the function $g(E; e) = E - e\sin E$ (cf. 3) in more detail. In particular, we note that for $E \in (0, \pi)$:

$$0 < \sin E < 1 \quad \Rightarrow \quad E - e < g(E; e) < E. \tag{6}$$

Given that our solution requires $g(E^*(\ell, e); e) = \ell$, we find the bound $E_*(\ell, e) \in (\ell, \ell + e)$ for $\ell < \pi$, as shown in Fig. 1. Together, this motivates the contour $C = \{z: |z - (\ell + e/2)| = e/2\}$, i.e. a circle of radius $e/2$ centred at $\ell + e/2$. This is guaranteed to enclose z_0

[3]The notation $\mathcal{R}\backslash\{z_0\}$ indicates the set $\mathcal{R}$ excluding the point z_0.

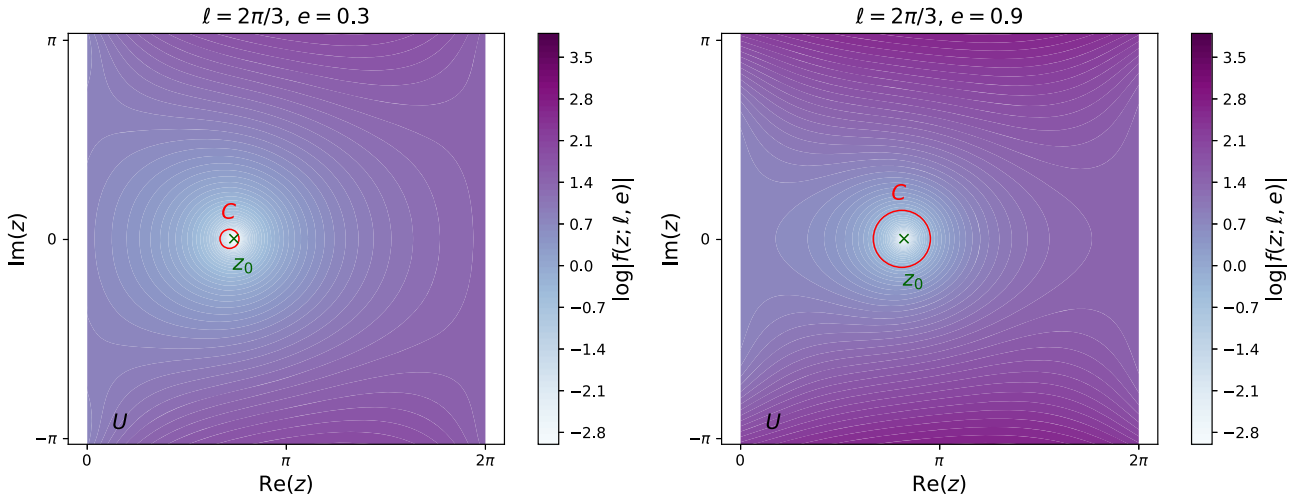

Figure 2. Plots of $f(z;\ell,e)$ (equation 4) in the complex plane, from which the integral solution (7) to Kepler's equation is obtained. The colourbar shows the value of $\log|f(z;\ell,e)|$ with the green $\times$ indicating z_0 such that $f(z_0;\ell,e)=0$, i.e. the desired solution. The coloured area indicates the open subset U upon which the result (5) is valid (denoted by the black U at lower left), and we evaluate the contour integrals on the closed curve C (in red), which is guaranteed to contain z_0. As proven in the text, z_0 is the sole zero of $f(z;\ell,e)$ in U. Note that the C encloses the region $E\in(\ell,\ell+e)$ on the real line in which the true solution certainly lies; its centre does not have to align with z_0 however. Here, we show the behaviour at $\ell=2\pi/3$ for two choices of eccentricity ($e=0.3$ and $e=0.9$), but all choices are qualitatively similar.

(ignoring the trivial case $\ell=\pi$), and is contained within U, since $e<\pi/2$.[4]

Given the above, we may apply (5) to our problem, obtaining the solution

$$E_*(\ell,e)\equiv z_0(\ell,e) = \left[\oint_C \frac{z\,\mathrm{d}z}{z-e\sin z-\ell}\right] \Big/ \left[\oint_C \frac{\mathrm{d}z}{z-e\sin z-\ell}\right]. \tag{7}$$

This may be straightforwardly inserted into (2) to obtain the Cartesian evolution of the orbit as a function of ℓ. For reference, we show the function $f(z;\ell,e)$ alongside the region U and the contour C in Fig. 2, for a representative choice of ℓ and e.

3 PRACTICAL EVALUATION

To obtain a simply implementable form of (7), we first parametrize the circular contour C by the function $\gamma\colon[0,1)\to C$ where $\gamma(x)=x_0+\Delta x\,e^{2\pi i x}$ for contour centre x_0 and radius Δx. As in Section 2, these are set to $x_0=\ell+e/2$, $\Delta x=e/2$. Inserting this into (7) and changing variables leads to

$$E_*(\ell,e)=x_0+\Delta x\left[\int_0^1 \mathrm{d}x\,e^{4\pi i x}a(x;\ell,e)\,\mathrm{d}x\right] \Big/ \left[\int_0^1 \mathrm{d}x\,e^{2\pi i x}a(x;\ell,e)\right], \tag{8}$$

where we define

$$a(x;\ell,e)=1/f(\gamma(x);\ell,e) = 1/[x_0+\Delta x\,e^{2\pi i x}-\ell+e\sin(x_0+\Delta x\,e^{2\pi i x})]. \tag{9}$$

[4]An alternative bound is given by $E_*(\ell,e)\in(\ell,\min[\pi,\ell+e])$. Whilst this results in a tighter contour for $\ell>\pi-e$, it will not be applied in this work, since the associated circular contour has a radius dependent on ℓ, which hampers numerical efficiency (cf. Section 3), since the contour integrand is no longer separable in ℓ and the path-variable x. For further discussion on solution bounds see Serafin (1986, 1998).

Defining the Fourier series coefficients of $a(x;\ell,e)$ by

$$a_k(\ell,e)\equiv\int_0^1 \mathrm{d}x\,e^{-2\pi i k x}a(x;\ell,e), \tag{10}$$

for integer k, (8) can be written

$$E_*(\ell,e)=x_0+\Delta x\,\frac{a_{-2}(\ell,e)}{a_{-1}(\ell,e)}. \tag{11}$$

For any given ℓ or e, we can thus evaluate $E_*(\ell,e)$ by computing the integrals a_{-2} and a_{-1}. In general, these must be evaluated numerically. One option for this (advocated for in Ullisch 2020 and Slepian & Philcox 2021) is to use a Fast Fourier Transform (FFT) to obtain all a_k frequencies simultaneously, for given ℓ, e. However, this is not the most efficient choice. The FFT algorithm scales as $N\log N$, for N grid-points; for computing N frequencies, this is clearly superior to computing N numerical integrals, but when only two are required (as here), the latter method is preferred. To expedite computation, we note that the real-part of each integral is symmetric around $x=0.5$ (with the imaginary part antisymmetric, and thus cancelling), giving

$$\begin{aligned} a_k(\ell,e) &= 2\int_0^{0.5}\mathrm{d}x\,\mathrm{Re}[e^{-2\pi i k x}a(x;\ell,e)] \\ &\approx A\left(a(0;\ell,e)+(-1)^k a(0.5;\ell,e)\right. \\ &\quad\left.+\sum_{j=1}^{N-1}\mathrm{Re}[e^{-2\pi i k j}a(0.5\,j/N;\ell,e)]\right), \end{aligned} \tag{12}$$

where we have approximated the integral by a discrete sum of N points in the second line, for some normalization constant A which will cancel in (11) when we take the ratio. Furthermore, we may compute the real parts explicitly and thus avoid any invoking complex numbers in the implementation of (12), again leading to faster computation. Alternative numerical methods such as Goertzel's algorithm (Goertzel 1958) may also be used to approximate these integrals.

From (11), we see the utility of using a narrow contour C. If Δx is small (implying x_0 is close to the true solution, since the latter must be enclosed by C), then the second term of (11) must also be small. For a given desired accuracy in E_* one can thus use fewer grid-points N for the numerical integral in (12), obtaining a faster algorithm. This is borne out in practice, since the contour with $x_0 = \ell + e$ and $\Delta x = \pi/2$ is found to be much more accurate than $x_0 = \pi/2$, $\Delta x = \pi/2 - \epsilon$ (the analogue to that used in Slepian & Philcox 2021) for the same N.

In a typical setting, one may wish to compute the eccentric anomaly $E_*(\ell, e)$ for many values of ℓ (equivalently, time) simultaneously. In this case, computation can be expedited by pre-computing $\sin(-2\pi ikj)$ (which is independent of ℓ) for each $j = 1, ..., N-1$. Additionally, the factor $\sin\left(x_0 + \Delta x\, e^{2\pi i x}\right)$ appearing in (9) may be expanded as

$$\begin{aligned}\sin(x_0 + \Delta x\, e^{2\pi i x}) &= \sin(x_0 + \Delta x\, \cos 2\pi x)\cosh(\Delta x\, \sin 2\pi x)\\ &\quad + i\cos(x_0 + \Delta x\, \cos 2\pi x)\sinh(\Delta x\, \sin 2\pi x)\\ &= [\sin x_0 \cos(\Delta x\, \cos 2\pi x)\\ &\quad + \cos x_0 \sin(\Delta x\, \cos 2\pi x)]\cosh(\Delta x \sin 2\pi x)\\ &\quad + i[\cos x_0 \cos(\Delta x\, \cos 2\pi x)\\ &\quad - \sin x_0 \sin(\Delta x \cos 2\pi x)]\sinh(\Delta x \sin 2\pi x).\end{aligned} \tag{13}$$

Whilst elementary, this is none the less useful. With our choice of contour, $x_0 \equiv x_0(\ell, e)$, $\Delta x \equiv \Delta x(e)$, with neither depending on x. This implies that the factors $\sin x_0$, $\cos x_0$ are independent of x (and hence N), thus must be computed only once per integral evaluation. Since Δx is independent of ℓ, every other function appearing in (13) needs to be computed only once per sampling point, even if a large array is used. This reduces the number of trigonometric function evaluations from $N_\ell \times (N-1)$ to $N_\ell + N - 1$, where N_ℓ is the size of the input ℓ array, and we note that the points $x = 0$ and $x = 0.5$ are trivial. Once the functions appearing in (13) are pre-computed, (12) requires only addition and multiplication operations, thus is highly efficient.

4 ALTERNATIVE METHODS

Before presenting the results of our approach, we discuss several popular alternatives. Further details on these can be found in Murray & Dermott (1999) and Danby (1988).

4.1 Series solutions

To obtain an iterative solution to (1), we first assume the eccentricity to be small, giving the zeroth-order solution $E_0(\ell, e) = \ell$. Inserting this into the Kepler equation leads to the first-order solution $E_1(\ell, e) = \ell + e\sin\ell$, which may be re-inserted to obtain a second-order solution, et cetera. Taking the infinite limit, this can be written as a Fourier series

$$E_*(\ell, e) = \ell + 2\sum_{s=1}^{\infty} \frac{1}{s} J_s(se)\sin s\ell, \tag{14}$$

(Murray & Dermott 1999), where $J_n(x)$ is a Bessel function of the first kind of the order of n. In practice, we can only compute a finite number of terms; truncating at $s = s_{\rm max}$ incurs an error scaling as $e^{s_{\rm max}+1}$, which, for small e, can be made negligible. As shown in Hagihara (1970), the series converges very slowly at large e due to the singularity of Kepler's equation at $e = 1$, $\ell = 0$; the utility of this approach is thus limited in such regimes.

To implement (14), one must compute the Bessel coefficients for each order s up to $s_{\rm max}$. Since these are independent of ℓ, they may be pre-computed for speed (assuming e is fixed), implying that the algorithm requires only $N_\ell \times s_{\rm max}$ trigonometric function evaluations to compute solutions for a grid of N_ℓ mean anomalies.

4.2 Numerical solutions

A common means of solving monotonic equations such as (1) is with root-finding, for example via the quadratic Newton–Raphson (NR) method or the quartic approach of Danby (1988). For this, one first defines

$$h(E; \ell, e) = E - e\sin E - \ell \tag{15}$$

with $h = 0$ at the desired solution. The iterative solutions are given by

$$\begin{aligned}E_{i+1}^{\rm NR}(\ell, e) &= E_i(\ell, e) + \delta_{i1}\\ E_{i+1}^{\rm Danby}(\ell, e) &= E_i(\ell, e) + \delta_{i3}\end{aligned} \tag{16}$$

for $i = 0, 1, 2, ...$, using the definitions

$$\begin{aligned}\delta_{i1} &= -\frac{h_i}{h_i'}, \quad \delta_{i2} = -\frac{h_i}{h_i' + (1/2)\delta_{i1}h_i''}, \quad \delta_{i3}\\ &= -\frac{h_i}{h_i' + (1/2)\delta_{i2}h_i'' + (1/6)h_i'''\delta_{i2}^2}\end{aligned} \tag{17}$$

for $h_i \equiv h(E_i; \ell, e)$. These require the derivatives $h'(E; \ell, e) = 1 - e\cos E$ et cetera, which are inexpensive to compute given $\sin E$ and $\cos E$. In total, the method requires two trigonometric function evaluations each step, (or $2N_\ell N_{\rm step}$ in total across $N_{\rm step}$ iterations) as well as a number of (cheap) multiplications and additions.

Both the Newton–Raphson and Danby prescriptions require also the initial condition, $E_0(\ell, e)$. Here, we adopt the method of Danby (1988), with

$$E_0(\ell, e) = \ell + 0.85e, \tag{18}$$

but note the additional discussion in Danby (1987), Calvo et al. (2013), and Elipe et al. (2017). In particular, the first work notes that convergence to one part in 10^{12} can be achieved for all allowed ℓ and e values with a maximum of three iterations. We note that a similar procedure is given in Markley (1995), setting the initial step equal to the solution of a cubic, then performing a single fifth-order root-finding step. Whilst highly accurate, it is not arbitrarily so, and is thus not considered in this work.

5 DISCUSSION

We now compare our prescription (Sections 2 and 3) to the well-known techniques of Section 4. For testing, we generate a grid of 10^6 equally spaced points in eccentric anomaly E (defining the 'ground truth' solution) and compute the mean anomaly ℓ for each via (1), assuming e to be fixed. Fig. 3 compares the results from our method (using 10^3 grid-points) with the truth for two choices of eccentricity e and various numbers of grid-points, N. The results are as expected: the error in the approach falls strongly with increasing N,[5] with accuracy of machine precision achieved for most ℓ at $N = 8$ ($N = 16$)

[5]The error decreases exponentially with increasing N at fixed e because the error is due to aliasing of higher frequency Fourier harmonics, and because harmonics of analytic functions fall exponentially at rates proportional to the distance from the integration contour to the nearest singularity.

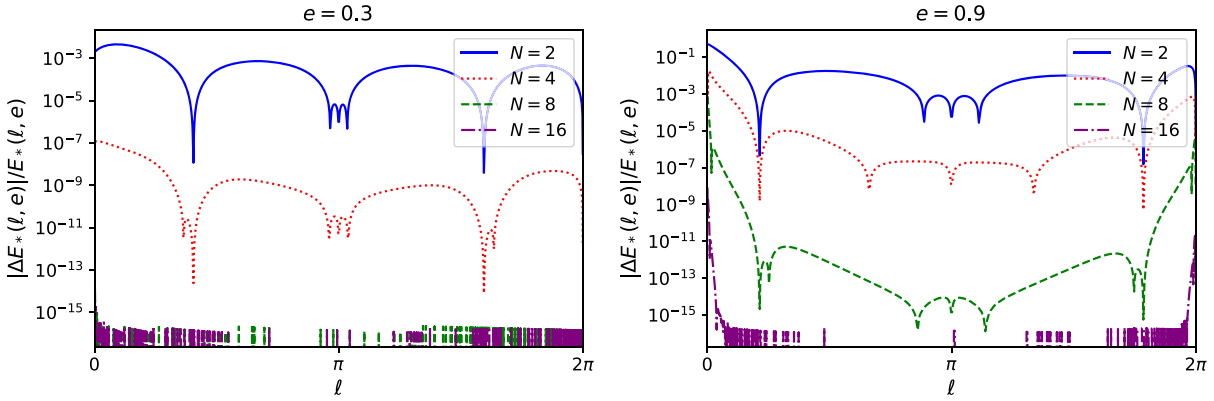

Figure 3. Accuracy of the contour-integration approach to Kepler's equation. Results are shown for two choices of eccentricity e, varying the mean anomaly ℓ, and the number of integration points N and plotting the quantity $|\Delta E_*(\ell, e)|/E_*(\ell, e) \equiv \left|E_*^{\rm true}(\ell, e) - E_*^{\rm contour}(\ell, e)\right|/E_*(\ell, e)$. This uses 10^3 points in ℓ, generated from an equally spaced grid in E (giving the true solution). The region $\ell > \pi$ can be obtained from $\ell < \pi$ by symmetry, but we include it here for completeness. As expected, the error in the contour integration decreases rapidly as N increases, and is somewhat larger for greater e, due to a wider contour C, as in Fig. 2. An additional plot of the error, including its dependence on e, is shown in Fig. 4. As shown in Table 1, our approach requires less computation time relative to that of conventional methods when the desired precision is held constant.

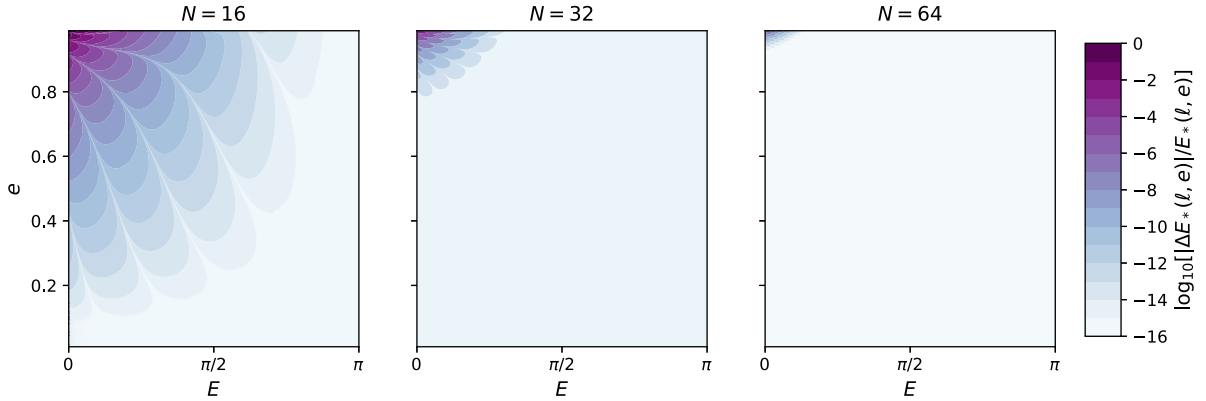

Figure 4. Fractional error in the contour-integration method as a function of eccentricity e and true eccentric anomaly E. We plot the logarithm of the error (defined as in Fig. 3) for three choices of integration step N, and show only results for $E < \pi$. 10^3 points in both e and E (and thus ℓ) are used to generate this figure. Moving towards the singularity at $e = 1$, $\ell = 0$, the error increases, but is greatly reduced by choosing a larger N.

for $e = 0.3$ ($e = 0.9$). Furthermore, we find a generally larger error at higher e: this is expected since the radius of the integration contour is proportional to e, and the solutions lie further from the line $E = \ell$, as in Fig. 1. This is further explored in Fig. 4, whereupon the error is shown to increase as one moves towards the singularity at $e = 1$, $\ell = 0$. Increasing the number of grid-points greatly reduces this however, highlighting the importance of choosing N appropriately.

To place our method in context, we compare it to the three alternative prescriptions (series, Newton–Raphson, and Danby) discussed in Section 4. For this purpose, we implement each in C++, paying close attention to efficiency.[6] To ensure each method has a similar level of accuracy, we gradually increase the precision of each method (either by increasing the number of grid-points in the numerical integral, or the number of iterations) until a mean absolute precision of 10^{-12} is obtained relative to the 'ground-truth' solution.

The final hyperparameter values and runtimes for the $N_\ell = 10^6$ array of mean anomalies are shown in Table 1 for three values of the eccentricity. As expected, both the Newton–Raphson and Danby methods converge quickly, with the latter requiring a maximum of three iterations even at the most extreme case of $e = 0.9$. The Danby prescription requires more computational operations per iteration, thus its runtime is only slightly reduced relative to Newton–Raphson, despite the fact that the number of iterations is roughly halved.

[6]C++ code implementing all of these can be found at github.com/oliverphilcox/Keplers-Goat-Herd.

Table 1. Computation time (in milliseconds) required to solve Kepler's equation (1) for 10^6 ℓ points (equally spaced in E) using three popular methods and that of this work. The Newton–Raphson and Danby (1988) methods are quadratic (quartic) root-finders, whilst the series approach is an expansion in eccentricity. The number of iterations (or integration points) $N_{\rm it}$ was chosen by repeating the calculation until a mean absolute error below 10^{-12} (relative to the true solution) was obtained for the sample. All algorithms were implemented in C++ and run on a 2019 MacBook Pro with a 6-core 2.6 GHz Intel i7 processor. The series was very slow to converge for $e = 0.9$, hence no timings are shown. We find our approach to be significantly faster than the alternatives considered.

Method	$e = 0.1$		$e = 0.5$		$e = 0.9$	
	$N_{\rm it}$	Time	$N_{\rm it}$	Time	$N_{\rm it}$	Time
Newton–Raphson	3	97.5	4	133	5	192
Danby (1988)	2	82.8	2	82.8	3	127
Series	11	116.2	47	516	–	–
This Work	**5**	**35.1**	**7**	**41.1**	**18**	**65.9**

Significantly more iterations are required for the series solution of (14), particularly as e increases. Given its nature as a perturbative solution, this is unsurprising, and we conclude that it is of most use only for orbits of very low eccentricity. Finally, we consider our approach. In all cases, we require $N \leq 18$ grid-points in the numerical integral (with N rising as e increases, as in Fig. 2), and find that the computation time is significantly reduced (by a factor ~ 2–3) compared to any of the alternative prescriptions. This may be understood by considering the number of trigonometric operations involved: assuming $N_\ell \gg N$, the total is proportional to N_ℓ, and thus independent of the number of steps. Each integration step simply requires multiplication and addition operations, giving a faster speed.

To summarize, this work demonstrates that new methods to solve the Kepler equation can provide solutions outperforming those of established methods over a wide range of parameter space. Our approach is based on contour integration, using methods developed to solve the 'geometric goat problem' in Ullisch (2020) and recently applied to the dynamics of spherical collapse in Slepian & Philcox (2021). We expect such approaches to be similarly applicable to other problems that require the solution of transcendental equations.

ACKNOWLEDGEMENTS

We thank Tom Dickens, Hanno Rein, Ian Weaver, and the Twitterverse for insightful feedback. We are additionally grateful to the referee, Manuel Calvo, for an insightful report. OP acknowledges funding from the WFIRST program through NNG26PJ30C and NNN12AA01C.

DATA AVAILABILITY

The data underlying this article will be shared on reasonable request to the corresponding author. C++ and PYTHON implementations of our code are available at github.com/oliverphilcox/Keplers-Goat-Herd.

REFERENCES

Calvo M., Elipe A., Montijano J. I., Rández L., 2013, Celest. Mech. Dyn. Astron., 115, 143
Colwell P., 1993, Solving Kepler's Equation over Three Centuries. Willmann-Bell, Richmond, Virginia
Danby J. M. A., 1987, Celest. Mech., 40, 303
Danby J. M. A., 1988, Fundamentals of celestial mechanics. Willmann-Bell, Richmond, Virginia
Elipe A., Montijano J. I., Rández L., Calvo M., 2017, Celest. Mech. Dyn. Astron., 129, 415
Goertzel G., 1958, Am. Math. Monthly, 65, 34
Hagihara Y., 1970, Celestial Mechanics. Vol.1: Dynamical Principles and Transformation Theory. MIT Press, Cambridge, MA
Jackson D., 1916, Ann. Math., 17, 172
Jackson D., 1917, Ann. Math., 19, 142
Kepler J., 1609, Astronomia Nova Aitiologetos, Seu Physica Coelestis, tradita commentariis De Motibus Stellæ Martis, Ex observationibus G. V. Tychonis Brahe.
Luck R., Stevens J. W., 2002, SIAM Rev., 44, 227
Luck R., Zdaniuk G., Cho H., 2015, Int. J. Eng. Math., 2015, 523043
Markley F. L., 1995, Celest. Mech. Dyn. Astron., 63, 101
Murray C. D., Dermott S. F., 1999, Solar System Dynamics. Cambridge Univ. Press, Cambridge
Serafin R. A., 1986, Celest. Mech., 38, 111
Serafin R. A., 1998, Celest. Mech. Dyn. Astron., 70, 131
Siewert C. E., Burniston E. E., 1972, Celest. Mech., 6, 294
Slepian Z., Philcox O. H. E., 2021, preprint (arXiv:2103.09823)
Ullisch I., 2020, Math. Intell., 42, 12

This paper has been typeset from a TEX/LATEX file prepared by the author.